JOURNAL OF SPACECRAFT AND ROCKETS
Vol. 34, No. 1, January–February 1997

Damped Oscillations of a Liquid/Gas Surface upon Step Reduction in Gravity

G. Wölk,* M. Dreyer,† and H. J. Rath‡
University of Bremen, 28359 Bremen, Germany
and
M. M. Weislogel§
NASA Lewis Research Center, Cleveland, Ohio 44135

The reorientation and settling of a liquid/gas interface in a right circular cylinder upon step reduction in gravity is investigated numerically. A modified dynamic contact angle boundary condition is implemented where the hysteresis parameter γ is employed as an adjustable parameter representing the degree of relative slip at the contact line. The effect of the boundary condition on the axial interface oscillation is studied and the dependence thereon of the resonant frequency and settling time is given. Results are shown regarding the behavior of the dynamic contact angle and the penetration of the surface oscillations into the bulk liquid. The numerical results are tuned via comparisons with existing experimental data, and a method for estimating the appropriate boundary condition providing good agreement is suggested. An accompanying scale analysis depicts γ as a function of the Ohnesorge number, the cylinder radius, and the static contact angle. These independent parameters are measures of the system damping, characteristic surface deflection, and effective stiffness of the interface. Applications of the results may be made to spacecraft fluids management and the use of spacecraft and/or drop towers for fluids experimentation.

Nomenclature

Bo = Bond number
Ca = capillary number
D = damping rate
g = acceleration level, cm/s^2
H = height of the liquid along the centerline of the cylinder at $t = 0$ (see Fig. 2), cm
H_∞ = height defined in Fig. 2, cm
H_0 = distance of centerline coordinate between its initial and final value (see Fig. 2), cm
$\mathcal{H}$ = mean curvature of the interface, cm^{-1}
h = free surface elevation, cm
h_∞ = low-g equilibrium height of the contact line at the wall (see Fig. 2), cm
L = characteristic surface dimension, cm
Oh = Ohnesorge number
p, p_a = fluid and ambient gas pressure, g/cm-s^2
R = radius of the cylinder, cm
Re = Reynolds number
$\boldsymbol{R}_i$, $\boldsymbol{R}_0$ = residual force vector at iteration i and for the solution of the previous time step, respectively
r = radial coordinate, cm
t = time, s
t_s = settling time, s
$t_{s,\exp}$ = settling time evaluated from experiment, s
U = characteristic system velocity, cm/s
$\boldsymbol{U}_i$ = solution vector at iteration i
u_r, u_z = velocity components, cm/s
$\boldsymbol{u}$ = velocity vector
V = capillary velocity scale, cm/s
z = axial coordinate, cm
γ = hysteresis coefficient, cm^{-1}
γ_0, γ_{real} = hysteresis coefficient from scaling and from comparison to experimental results, respectively, cm^{-1}
Δh_0 = height difference, cm
θ_{stat}, θ_d = static and dynamic contact angle, respectively, deg
μ = fluid dynamic viscosity, g/cm-s
ρ = fluid density, g/cm^3
σ = surface tension, g/s^2
τ = time constant, s
τ_n, τ_t = normal and tangential stress at fluid interface, g/cm-s^2
ω_r = resonant frequency, Hz
$\omega_{r,\exp}$ = resonant frequency of experimental results, Hz

Introduction

FOR fluid systems with free interfaces, the competition between gravitational forces and surface tension forces is usually expressed through the Bond number

$$Bo = \frac{\Delta\rho g L^2}{\sigma} \tag{1}$$

In cases where $Bo \ll 1$, the effects of gravity are small in comparison to those of surface tension and capillary dominated systems result. On Earth, such conditions are typically achieved in systems of small length scale $L \lesssim O$ (1 mm). In the near weightlessness of space, however, g may be reduced by many orders of magnitude, and in such environments dominance of capillary forces ($Bo \ll 1$) over large length scales is commonplace. This fact dramatically impacts the design of in-space fluid systems and demands a thorough understanding of capillary dominated phenomena.

Unfortunately, the complexity of such large-scale free surface flows can be extreme, an example being spacecraft liquid storage tanks. In most cases, real space fluid systems have complicated geometries and require transient three-dimensional nonlinear analyses, the latter owing in part to the conditions required for specifying the moving and highly deformable interface. Numerical analysis is often the only recourse for quantitative analysis. Though a number of investigators have written or adapted computer codes to handle problems of moving interfaces with predominant capillary forces,

Received April 25, 1996; revision received Aug. 23, 1996; accepted for publication Sept. 13, 1996.

*Research Scientist, Interface Phenomena Branch, Center of Applied Space Technology and Microgravity.
†Group Manager, Interface Phenomena Branch, Center of Applied Space Technology and Microgravity.
‡Professor, Department of Mechanical Engineering, Center of Applied Space Technology and Microgravity.
§Aerospace Engineer, Microgravity Fluids Branch.

it is not often possible to buttress their results against experimental data due to its scarcity. (Appropriate numerical and theoretical examples for this study may be found in Refs. 1 and 2. For recent advances in solution algorithms for free surface problems, see Ref. 3 and references contained therein.) This deficiency is perhaps most disturbing for numerically analyzed systems that possess a moving contact line—the three phase line of contact where the free interface intersects the container wall. Since the boundary condition at the contact line is not fully understood[4] from a physical point of view, an ad hoc condition is often employed by default. The particular selection of this boundary condition can be critical since many low-g free surface problems are dominated by both interfacial curvature and damping originating at the contact line.[5] It is the purpose of this study to demonstrate yet another approach to the practical modeling of the contact line boundary condition for an oscillating free surface problem, which may prove useful in future numerical investigations.

In this study a "test" problem is investigated numerically for which experimental data are available for subsequent comparisons. The particular problem selected concerns the reorientation and settling (damped oscillations) of a fluid meniscus in a right circular cylinder upon a step reduction in gravity level. This reorientation is a common occurrence in drop towers where after release of the experiment package the fluid systems undergo a rapid change from the gravity dominated ($Bo \gg 1$) to the capillary dominated ($Bo \ll 1$) regime. This test problem also provides insight into applications including docking maneuvers of liquid fuel laden spacecraft, the behavior of liquid propellants upon termination of thruster firing, and the general settling characteristics of fluid interfaces that are disturbed by spurious accelerations (g-jitter). As is the case for the partially fluid–filled cylinder, depending on the fluid-solid contact angle, the fluid moves from an essentially flat surface configuration to that of a spherical cap (Fig. 1). Though the process appears at first glance quite simple, the interplay between the moving contact line, the static contact angle, the cylinder radius, and the fluid properties is indeed intricate. As might be expected, overdamped or underdamped behavior of the interface depending on the magnitude of the damping and restoring forces of the system is possible. An important dimensionless number for this problem, somewhat analogous to the damping ratio in the spring-mass-damper system, is the Ohnesorge number

$$Oh = \mu/\sqrt{\rho\sigma L} \tag{2}$$

where Oh is the square root of the ratio of unsteady to viscous time scales in capillary dominated systems. In this case, the quantity Oh^{-2} is equivalent to the Reynolds number ($Re = VR/\nu$), where the capillary velocity scale $V \sim \sigma/\mu$ is chosen. [The particular relationship between Reynolds and Ohnesorge numbers depends on the selection of the velocity scale V. For example, see Ref. 6, where $V \sim (\sigma/\rho R)^{1/2}$ and thus $Re \sim Oh^{-1}$.] With a step reduction in gravity for $Oh \gg 1$, the fluid gradually creeps to its end state configuration, whereas when $Oh \ll 1$ the fluid overshoots this state and experiences damped axial-mode oscillations until equilibrium is established. In this numerical study, Ohnesorge numbers in the range of $0.00146 \leq Oh \leq 0.0440$ are investigated, as these were also studied experimentally by Weislogel and Ross.[7] A commercial code is employed for the computations with a modified dynamic contact angle boundary condition at the contact line. A hysteresis parameter γ arises as an adjustable parameter for the numerical calculations through which to establish quantitative agreement with experiment. With this knowledge, γ may be correlated with the independent variables of the problem and thus form an approximate numerically empirical method of predicting the correct boundary condition for related flows. Results of the dependence of the natural frequency and the settling time for the fluid reorientation on γ are presented in detail.

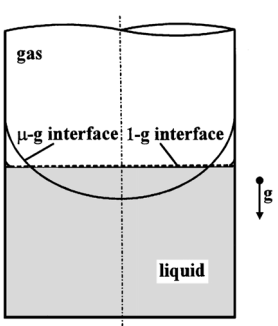

Fig. 1 Normal and low-gravity interfacial surfaces in a right circular cylinder.

Background and Approach

A number of applicable experimental studies have been performed concerning surface reorientation and oscillation in low-gravity environments.[7–9] Most recently, Weislogel and Ross[7] studied the reorientation of different liquids in a right circular cylinder. A variety of silicone oils were used, which allowed the variation of the dynamic viscosity without significant variation of other relevant fluid properties. A range of contact angles was achieved by varying the wetting characteristics of the test containers with surface coatings applied to the cylinder walls. Damped oscillations of a liquid/gas interface were shown to be dependent primarily on the Ohnesorge number and the static contact angle θ_{stat}. Since the Ohnesorge number would appear as a parameter in the governing nondimensionlized Navier–Stokes equation for this problem, $Re \sim 1/Oh^2$, its effects on the flow will be accounted for naturally in any numerical investigation. However, the treatment of the contact line or contact angle condition at the wall is uncertain, particularly in the case of unsteady, intermediate to high Reynolds number flows. For unidirectional flows, as discussed in Ref. 4, there exists a clear relationship between the contact angle and the contact line velocity at low Reynolds numbers (high Ohnesorge numbers). For oscillating contact line conditions, Young and Davis[10] propose four model relationships between the contact angle and contact line velocity. These are 1) the fixed contact line, 2) the fixed contact angle, 3) the smooth contact angle variation, and 4) the contact angle variation incorporating contact line hysteresis (advancing/receding limits). Several of these conditions applied in numerical investigations may serve well to bracket the anticipated behavior of the fluid. For recent developments see Refs. 5, 11, and 12. In this investigation, a relationship established by Satterlee and Reynolds[13] for an inviscid laterally sloshing interface is adopted combining the effects of 1–3. The contact line conditions are represented by a linear boundary condition incorporating a hysteresis parameter that indicates the degree of contact angle fluctuation and contact line motion. Similar numerical investigations using the hysteresis parameter were conducted recently by Chao et al.[14] and Kamotani et al.,[6] who studied the viscid lateral sloshing problem for an initially flat interface ($\theta_{\text{stat}} = 90$ deg). A modification is made here to this condition to account for static contact angles other than 90 deg.

Equations and Boundary Conditions

A description of the dimensional mathematical model follows. Axisymmetry is assumed, and the coordinates (r, z) are sufficient to describe the velocity components $\boldsymbol{u}(u_r, u_z)$. The radius of the cylinder is $R = 0.9525$ cm (Ref. 7), and the height of the liquid at the centerline of the cylinder at the time $t = 0$ is $H = 2.0$ cm ($H \approx 2R$). The geometry is depicted in Fig. 2. The fluid is assumed to be incompressible and Newtonian with a passive overlying gas phase. The fluid properties used in the calculations are taken from Ref. 7 and are listed in Table 1.

The calculation begins with a liquid/gas interface shape determined for the normal gravitational field using a Runge–Kutta algorithm following Concus.[15] The initial condition is the surface

Table 1 Relevant fluid properties for silicone oil test fluids

ρ, g/cm^3	μ, g/cm-s	σ, g/s^2	θ_{stat}, deg	Oh
0.760	0.00494	15.9	32	0.00146
0.816	0.00818	17.4	44	0.00222
0.872	0.01744	18.7	51	0.00442
0.913	0.04565	19.7	59	0.0110
0.935	0.0935	20.1	60	0.0221
0.949	0.1898	20.6	66	0.0440

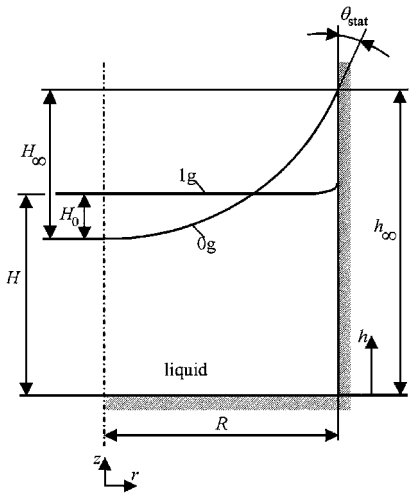

Fig. 2 Geometry and boundary conditions for the problem of surface reorientation in a right circular cylinder.

calculated for normal gravity ($1\,g = 981$ cm/s^2) instantaneously subjected to a zero gravity environment ($0\,g$) at a time $t = 0^+$. Thus, the body force term is not considered in the numerical calculations other than to determine the initial condition of the surface. The continuity and Navier–Stokes equations solved are

$$\frac{1}{r}\frac{\partial}{\partial r}(ru_r) + \frac{\partial u_z}{\partial z} = 0 \tag{3}$$

$$\rho\left(\frac{\partial u_r}{\partial t} + u_r\frac{\partial u_r}{\partial r} + u_z\frac{\partial u_r}{\partial z}\right) = -\frac{\partial p}{\partial r} + \mu\left(\frac{\partial^2 u_r}{\partial r^2} + \frac{1}{r}\frac{\partial u_r}{\partial r} - \frac{u_r}{r^2} + \frac{\partial^2 u_r}{\partial z^2}\right) \tag{4}$$

$$\rho\left(\frac{\partial u_z}{\partial t} + u_r\frac{\partial u_z}{\partial r} + u_z\frac{\partial u_z}{\partial z}\right) = -\frac{\partial p}{\partial z} + \mu\left(\frac{\partial^2 u_z}{\partial r^2} + \frac{1}{r}\frac{\partial u_z}{\partial r} + \frac{\partial^2 u_z}{\partial z^2}\right) \tag{5}$$

respectively. The boundary conditions for the preceding system are as follows: no slip along the wetted walls and the cylinder base; $\boldsymbol{u} = 0$ on $z = 0$, and, except in the near vicinity of the contact line, $\boldsymbol{u} = 0$ on $r = R$, the symmetry condition at the centerline, namely, $u_r = 0$ on $r = 0$, and normal and tangential stress components on the interface,

$$\tau_n = 2\sigma\mathcal{H} - p_a \tag{6}$$

$$\tau_t = 0 \tag{7}$$

where the ambient pressure p_a in the gas is set to zero. The kinematic condition at the surface $h(r, t)$ is described by

$$u_z = \frac{\partial h}{\partial t} + u_r\frac{\partial h}{\partial r} \tag{8}$$

Because the interface is a surface of revolution about the z axis, a convenient expression for the mean curvature is

$$2\mathcal{H} = \frac{ff'' - (1 + f'^2)}{f(1 + f'^2)^{\frac{3}{2}}} \tag{9}$$

where $f = f(z)$ describes the free interface. Two boundary conditions for f must be specified for closure. These boundary conditions are given indirectly as the symmetry condition at $r = 0$ and the contact angle condition at the contact line. The boundary conditions for the free liquid surface are, at $r = 0$,

$$\frac{\partial h}{\partial r} = 0 \tag{10}$$

and at $r = R$,

$$\frac{\partial h}{\partial r} = \gamma(h - h_\infty) + \cot(\theta_{stat}), \qquad \text{for} \qquad \theta > 90\,\text{deg} \tag{11}$$

$$\frac{\partial h}{\partial r} = -\gamma(h - h_\infty) + \cot(\theta_{stat}), \qquad \text{for} \qquad \theta \le 90\,\text{deg} \tag{12}$$

The latter condition is a simple modification of the work of Satterlee and Reynolds[13] and Kamotani et al.,[6] which permits static contact angles other than 90 deg. The linearized condition is phenomenologically based and is readily incorporated into the solution algorithm as a description of the contact line boundary condition. The case $\gamma = 0$ corresponds to the fixed contact angle condition, whereas the condition $\gamma \to \infty$ is the pinned interface condition. The case $\gamma = 0$ allows slip at the contact line to preserve the contact angle there, whereas in the case of the latter, the contact line moves rapidly from its initial position toward h_∞ where it closely remains with the surface fluctuations near the wall being described by fluctuations mainly of the contact angle. For the intermediate range of γ, the effective dynamic contact angle varies smoothly with the height of the contact line.

Scale Analysis

As a consequence of the modeling choice $\gamma = \text{const}$, γ becomes a free parameter in the numerical calculations. Since γ may thus be tuned to provide agreement with experimental data, some a priori knowledge of the order of magnitude of γ is helpful and may be used as a guide for applications of the numerical technique to other geometries and/or fluid systems. Insight into the functional form of γ may also allow correlation with the relevant parameters of the problem providing intermediate, and more precise, predictions of fluid behavior as compared with the bounding predictions anticipated using $\gamma = 0$ and ∞.

A scale analysis is effective to this end. Defining $\partial h/\partial r = \cot(\theta_d)$ at $r = R$, with θ_d serving as an apparent dynamic contact angle, the boundary condition of Eq. (12) may be rearranged to give

$$\gamma = \frac{\cot(\theta_{stat}) - \cot(\theta_d)}{\Delta h} \tag{13}$$

where $\Delta h = h - h_\infty$. If γ is an authentic constant of the system, the time dependence of terms in the numerator and denominator must cancel. Therefore, only scale values for Δh and θ_d are necessary to gauge γ. Assuming $Bo(\text{initial}) \gg 1$, the difference Δh at $t = 0$ ($\equiv \Delta h_0$) may be determined using

$$\Delta h_0 = H_\infty - H_0 \tag{14}$$

The terms H_∞ and H_0 are depicted in Fig. 2. The height H_∞ is defined by

$$H_\infty = R\left[\frac{1 - \sin(\theta_{stat})}{\cos(\theta_{stat})}\right] \tag{15}$$

Conservation of fluid volume between 1 g and low-g states provides an additional relationship between H_0 and H_∞, namely,

$$\pi R^2 H_0 = \pi R^2 H_\infty - \pi H_\infty^2\left[\frac{R}{\cos(\theta_{stat})} - \frac{H_\infty}{3}\right] \tag{16}$$

Thus, upon substitution of Eqs. (15) and (16) into Eq. (14), Δh_0 may be approximated as

$$\Delta h_0 = \frac{R}{3\cos^3(\theta_{stat})}[2 + \sin(\theta_{stat})][1 - \sin(\theta_{stat})]^2 \tag{17}$$

The scale value for $\cot(\theta_{stat}) - \cot(\theta_d)$ may be estimated with insight into the magnitude of θ_d at the onset of the flow. The empirical expression of Jiang et al.[16] shows that for the advancing contact line

$$\theta_d = \arccos\left\{\cos(\theta_{stat}) - [1 + \cos(\theta_{stat})]\tanh(4.96Ca^{0.702})\right\} \tag{18}$$

The velocity scale of the capillary number may be determined using one-quarter of the period of oscillation determined by the inertial

Table 2 Range of γ, ω_r, and t_s for the silicone oils

Fluid properties		Scaling	Numerical results			Results from Ref. 7	
Oh	θ_{stat}	γ_0	γ_{real}	ω_r	t_s	$\omega_{r,exp}$	$t_{s,exp}$
0.00146	32	1.72	$\approx 100 \pm 30$	36.0[a]	2.70[a]	36.1	3.38[a]
0.00222	44	1.23	$\approx 70 \pm 20$	40.0[a]	2.50[a]	39.5	2.75[a]
0.00442	51	1.45	$\approx 100 \pm 30$	43.2	1.74	43.3	1.94
0.0110	59	2.09	$\approx 150 \pm 50$	46.1	1.12	46.3	1.62
0.0221	60	3.10	$\approx 200 \pm 20$	42.2	0.80	44.4	1.12
0.0440	66	4.48	$\approx 250 \pm 40$	43.1	0.57	44.3	0.66

[a]Linearly extrapolated value.

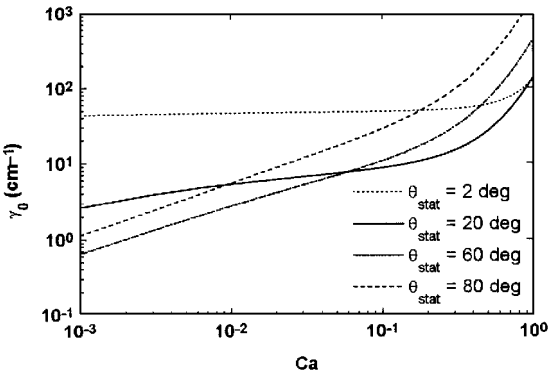

Fig. 3 Dependence of γ_0 on Ca as shown by Eq. (20) for cases of constant static contact angle θ_{stat} and constant cylinder radius (R = 0.9525 cm).

time constant $\tau \sim (\rho R^3/\sigma)^{1/2}$ for the period of oscillation of the interface. Thus $U \sim 4\Delta h_0/\tau$ is an applicable scale for the velocity of the contact line during the initial stages of the reorientation process. The capillary number based on this velocity is

$$Ca = 4(\Delta h_0/R)Oh \tag{19}$$

Substituting Eqs. (17–19) into Eq. (13), γ ($\equiv\gamma_0$) is evaluated and listed in Table 2 for several combinations of static contact angle and fluid properties, Bo(initial) $\gg 1$. Intermediate Bond numbers will alter the value of γ_0. For example, Bo(initial) ≈ 40 results in a +20% change in γ_0 as compared with the limit Bo(initial) $\to \infty$.

Thus, the scaling for γ reveals $\gamma = \gamma(\theta_{stat}, Ca, R)$ or $\gamma = \gamma(\theta_{stat}, Oh, R)$:

$$\gamma_0 \sim \frac{\cot(\theta_{stat}) - f(\theta_{stat}, Ca)}{f(\theta_{stat}, R)} \tag{20}$$

From Eq. (20), it can be shown that $\gamma_0 \sim 1/R$ and that $\gamma_0 \to \infty$ for both $\theta_{stat} \to 0$ and/or large capillary number. This behavior can also be observed in Fig. 3, where the dependence of γ_0 on the capillary number is plotted for cases of constant static contact angle θ_{stat} and constant cylinder radius (R = 0.9525 cm). If the capillary number is less than 0.1 and the value of θ_{stat} is in the range 0 deg $< \theta_{stat} <$ 2 deg, $\gamma_0 = \text{const} \sim \theta_{stat}$. It can also be shown that γ_0 increases with increasing capillary number ($Ca > 0.1$) for $\theta_{stat} > 2$ deg and that $\gamma_0 \to \infty$ as $\theta_{stat} \to 90$ deg. These features indicate the degree of effective slip or pinning at the contact line that might be anticipated for a given system of R, θ_{stat}, and Oh.

Numerical Considerations

The time-dependent response of the free liquid/gas interface to the step reduction in gravity level is computed using the finite element code FIDAP (Fluid Dynamics Package) (Ref. 17; version 7.5 was run). The fully transient Navier–Stokes equations are solved, generating quantitative results for comparison with experimental data. The only modification to the code is the boundary condition at the moving contact line, Eq. (11) or (12).

The code adopts a mixed velocity–pressure formulation. The basis element is a nine-node quadrilateral element. Within each element, the velocity components are approximated using a biquadratic interpolation function and the pressure is approximated using a linear interpolation function. From previous numerical investigations involving moving contact lines,[18,19] it is known that elements must become progressively smaller the nearer they are to the contact line. This condition was accomplished using a mesh refinement scheme. The smallest element is found directly at the point where the liquid/gas interface meets the wall. At $t = 0$, the dimensions are 0.002 cm in the r direction and 0.003 cm in the z direction. The standard mesh size of the computational domain is 73 radial nodes and 49 axial nodes. Finer mesh sizes produce results that are indistinguishable compared with this standard. The motions of two nodes are confined strictly to motion along the z direction. These nodes are located where the liquid/gas interface meets the wall and on the liquid/gas interface at the centerline. All others are free to adapt to the solution and so prevent undue distortion of the mesh. Application of the no-slip boundary condition at the contact line results in a stress singularity in problems where the contact line must move as a result of hydrodynamic forces.[20] The boundary conditions of Eqs. (11) and/or (12) relieve the stress singularity at the contact line by introducing a region of slip implemented into FIDAP.[17] The degree of slip (effective slip length) for the node at the wall during the first 10 time steps is in the range 7×10^{-5} to 9×10^{-5} cm.

The transient problem is computed with the implicit backward Euler integration scheme. At each time step a quasi-Newton method is used and iteration takes place when two convergence criteria are satisfied simultaneously:

$$\sqrt{\left(\frac{\boldsymbol{U}_i - \boldsymbol{U}_{i-1}}{\boldsymbol{U}_i}\right)^2} \leq 0.01 \tag{21}$$

and

$$\sqrt{(\boldsymbol{R}_i/\boldsymbol{R}_0)^2} \leq 0.01 \tag{22}$$

(for more details see Ref. 17). The initial time step for the first five time steps is 0.1×10^{-6} s, and thereafter a variable time increment is selected automatically by the code. The average run time was 900 min on a computer system of 512 MB RAM and 130.4 MFlops. The CPU time increases with increasing γ, decreasing Oh (holding θ_{stat} constant), and decreasing θ_{stat} (holding Oh constant) because the fluid motion requires more time to damp in these instances.

Results and Discussion

Surface Oscillation

With the step reduction in gravity from 1 g to low g, the fluid flows from a flat configuration toward its zero-g equilibrium shape. For the underdamped systems studied here, a damped oscillation of the fluid/gas interface about the low-g equilibrium configuration results. The behavior of the fluid depends on the value of γ for the contact line boundary condition. The principal objective was to determine the quantitative nature of the oscillations as a function of γ for systems of various Ohnesorge numbers and static contact angles in a similar manner to that of Chao et al.[14] and Kamotani et al.[6]

The effect of γ on the surface settling history may be best seen by observing the location of the meniscus centerline as shown in Fig. 4, where $Oh = 0.0110$ and $\theta_{stat} = 59$ deg. The data were obtained from the numerical results at each 10th time step. Figure 4 shows that, the higher the value of γ, the higher the oscillation amplitudes and the lower the damping. On close examination of the oscillation curves for $\gamma = 10$ and 100 cm^{-1}, one can see the presence of a higher frequency wave between $t = 0$ and the first minimum. To further illustrate the effect of γ on the computed interface behavior, Figs. 5–7 show the free surface shape for these three calculations, each from $t = 0$ to the first minimum. The impact of γ is distinct. From Figs. 5–7 it can be observed that a capillary wave is produced at the contact line that travels toward the centerline, causing a brief rise in the surface elevation there. This high-frequency wave becomes increasingly pronounced with increasing γ. It is also seen to decay rapidly as it gives way to the fundamental axial oscillations of the surface. Such a wave is often observed experimentally[9] and has been predicted in similar though inviscid computations.[2]

In contrast to Fig. 4, Fig. 8 is presented to illustrate the effect of γ on the location of the contact line ($r = R$) for the same fluid.

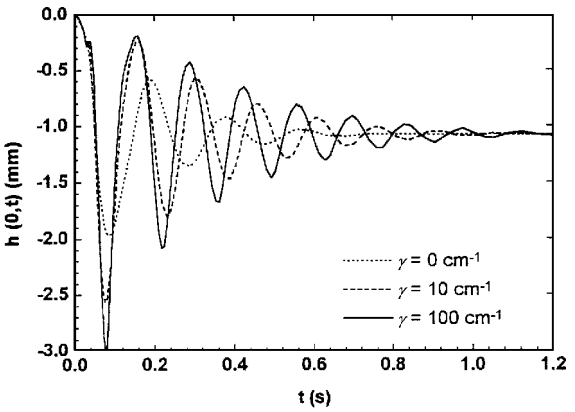

Fig. 4 Surface settling histories for $Oh = 0.0110$ at the cylinder centerline ($r = 0$) with $\theta_{stat} = 59$ deg and varying γ.

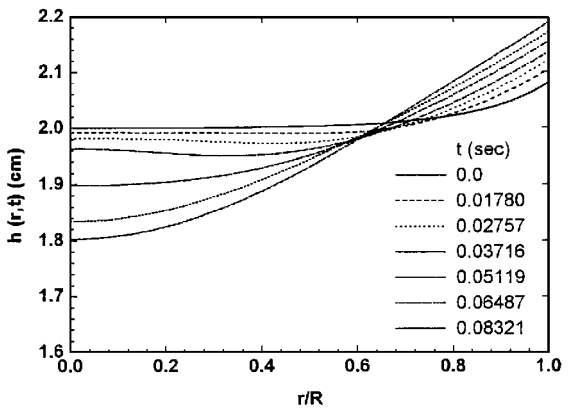

Fig. 5 Free surface shape for $Oh = 0.0110$ with $\theta_{stat} = 59$ deg for several time steps between $t = 0$ and the first minimum of the oscillation curve; $\gamma = 0$.

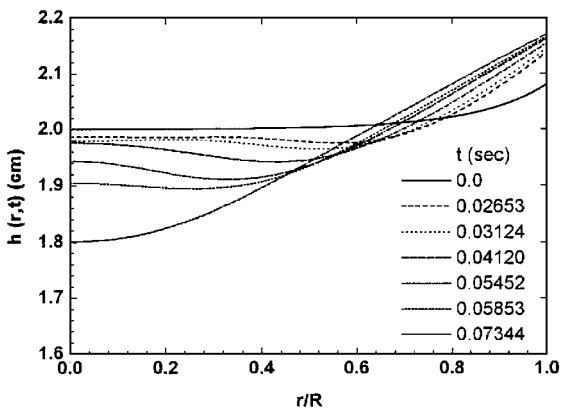

Fig. 6 Free surface shape for $Oh = 0.0110$ with $\theta_{stat} = 59$ deg for several time steps between $t = 0$ and the first minimum of the oscillation curve; $\gamma = 10$ cm^{-1}.

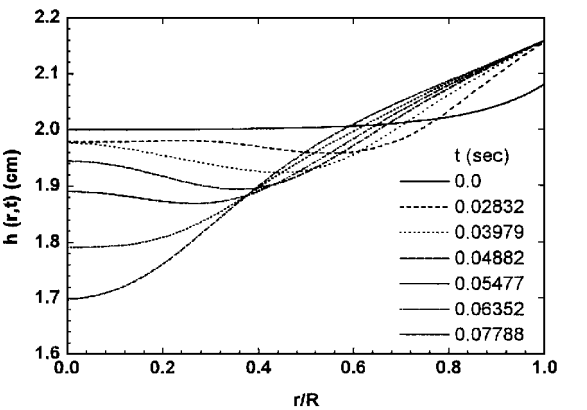

Fig. 7 Free surface shape for $Oh = 0.0110$ with $\theta_{stat} = 59$ deg for several time steps between $t = 0$ and the first minimum of the oscillation curve; $\gamma = 100$ cm^{-1}.

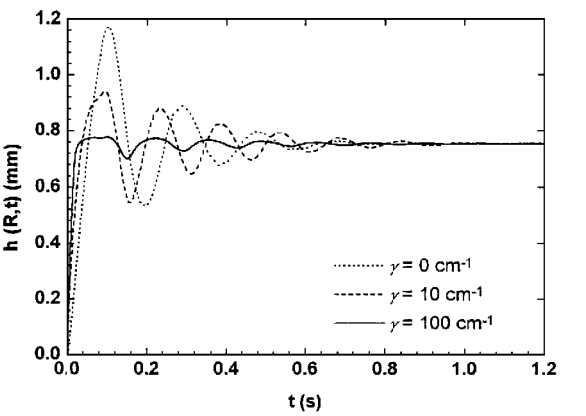

Fig. 8 Contact line settling histories for $Oh = 0.0110$ at the wall ($r = R$) for a variety of γ values with $\theta_{stat} = 59$ deg.

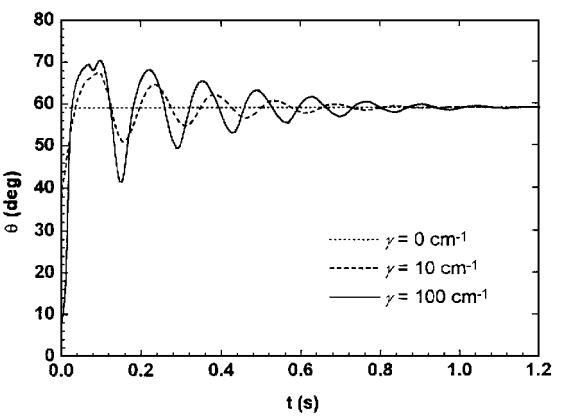

Fig. 9 Behavior of the dynamic contact angle for $Oh = 0.0110$ with $\theta_{stat} = 59$ deg and varying γ.

If $\gamma = 0$, the contact angle is fixed and the contact line is allowed to move without reservation. The result is an overshoot at the wall and a large-amplitude oscillation about the final value. If $\gamma = 100$ cm^{-1}, γ restrains the free movement of the contact line at the wall and oscillations of this point are weak.

Dynamic Contact Angle

The behavior of the dynamic contact angle θ_d with time for $Oh = 0.0110$ and a static contact angle $\theta_{stat} = 59$ deg is shown in Fig. 9. For $\gamma = 0$ the contact angle is fixed at the equilibrium value. However, for $\gamma > 0$ the calculation begins with a contact angle $\theta_d < \theta_{stat}$. The higher the value of γ, the smaller the initial value of θ_d. For example, $\theta_d = 36.4$ deg for $Oh = 0.0110$ and $\gamma = 10\,\text{cm}^{-1}$. For $\gamma = 100\,\text{cm}^{-1}$, $\theta_d = 7.0$ deg. This is an artifact of the boundary condition because, phenomenologically speaking, the dynamic contact angle does not decrease when the contact line is in an advancing state, but rather the contrary. The boundary condition is more representative after the first maximum, with θ_d increasing (decreasing) with advancing (receding) motion of the contact line. It can be seen that the θ_d maxima increase significantly with increasing γ and that there is appreciable unsteadiness during the first period of oscillation.

Resonant Frequency

It can be shown from the numerical results that the surface oscillations are not steady periodic. This behavior is due to the large nonlinear deflections of the interface experienced after reduction of g. As time passes, these deflections lessen and the surface oscillations and flow become more linear, leading eventually to steady periodic behavior. In general, the instantaneous frequency increases from a

lower to a higher steady value during the reorientation process. The degree of aperiodicity is dependent on the values of γ, θ_{stat}, and Oh. For high γ ($\gtrsim$50 cm^{-1}), θ_{stat} ($\gtrsim$59 deg), and Oh ($\gtrsim$0.0221), changes in the instantaneous frequency were detected up to 12%. However, for low γ ($\lesssim$50 cm^{-1}), lower θ_{stat} ($\lesssim$44 deg), and lower Oh ($\lesssim$0.00222), essentially steady periodic behavior was present with changes in frequency of less than 3% peak to peak. Steady periodic behavior (linear oscillations) can be expected when $\theta_{stat} \lesssim 51$ deg or when $Oh \lesssim 0.00222$ and in all cases when $\gamma \lesssim 10$ cm^{-1}. Changes in frequency for $\theta_{stat} < 51$ deg are in the range of 5% for $Oh < 0.0221$.

To make comparisons with the experimental results of Ref. 7, an average resonant frequency of the surface oscillations for the meniscus centerline for each calculation was determined in three different ways by curve fitting the surface settling histories at the meniscus centerline from $t = 0$ to the end, from the first maximum to the end, and from the second maximum to the end. The functional form used in the fit was

$$h(0, t) = H_0[\exp\{-Dt\}\cos(\omega_r t) - 1] \tag{23}$$

As might be anticipated from the preceding discussion, average frequencies that were determined using all nodes from the beginning ($t = 0$) to the end of the flow process had the highest standard error, whereas the average frequency values determined from the first and second maximum to the end were higher in magnitude. In the following discussion, we used for each calculation the frequencies with the smallest standard error value varying between 0.1 and 4.0%. Figures 10 (Oh = const) and 11 (θ_{stat} = const) show the dependence of the resonant frequency ω on the different contact line conditions. For every fluid, ω_r is minimized at $\gamma = 0$ and maximized as $\gamma \to \infty$. The change of ω_r from $\gamma = 0$ to $\gamma \to \infty$ lies in the range of 31–69%, and this change increases with increasing Oh and increasing θ_{stat}. As seen in Figs. 10 and 11, ω_r increases with

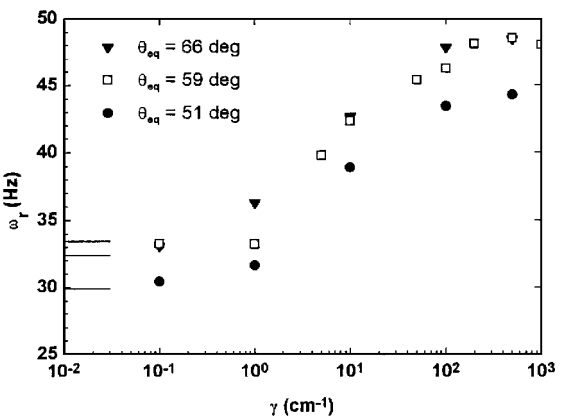

Fig. 10 Effect of γ on the resonant frequency ω_r for Oh = 0.0110 with varying equilibrium contact angle.

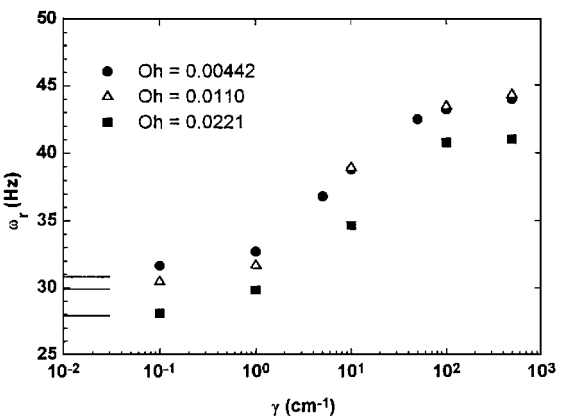

Fig. 11 Effect of γ on the resonant frequency ω_r for varying Ohnesorge number holding the equilibrium contact angle constant (θ_{stat} = 51 deg).

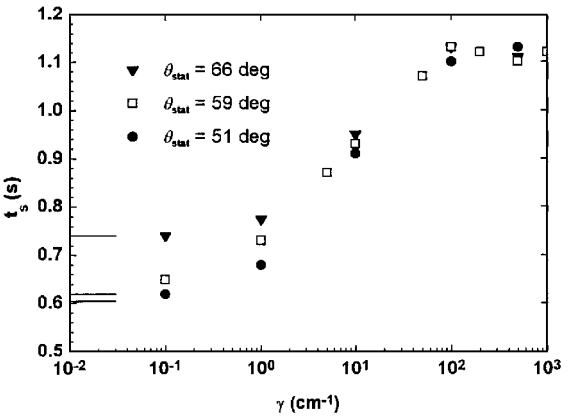

Fig. 12 Effect of γ on the settling time t_s for varying equilibrium contact angle; Oh = 0.0110.

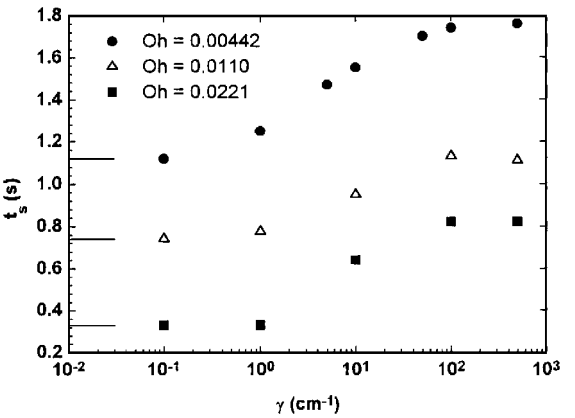

Fig. 13 Effect of γ on the settling time t_s for varying Ohnesorge number holding the contact angle constant (θ_{stat} = 51 deg).

increasing static contact angle and decreasing Ohnesorge number, respectively (for fixed γ). These trends were common to all calculations performed. The horizontal lines on the abscissa of such figures are the values of the function for $\gamma \to 0$.

Settling Time

The settling time t_s was defined as the time required for the surface oscillations to decay to 2% of the initial amplitude value. Figures 12 (Oh = const) and 13 (θ_{stat} = const) show the dependence of the settling time on γ for different contact angles and Ohnesorge numbers, respectively. On the abscissa are lines indicating the behavior of t_s for $\gamma \to 0$. In general, the settling time increases with increasing γ. It is seen that, for $\gamma \geq 100$ cm^{-1}, changes in the settling time with γ are weak and that as γ increases the settling time approaches a constant value similar to the resonant frequency. For every fluid the settling time is lowest at $\gamma = 0$ and highest for $\gamma \to \infty$. In contrast to the resonant frequency, the influence of the static contact angle on the settling time is weak for large γ. Pronounced changes in the settling time are only noticeable in the range 1 cm^{-1} $< \gamma <$ 100 cm^{-1}. Concerning the case of $\gamma = 0$, the change in the settling time between $\gamma = 0$ and $\gamma \to \infty$ lies in the range of 36–150%. Holding the contact angle constant in the range 51 deg $\leq \theta_{stat} \leq$ 66 deg, the settling time increases with decreasing Ohnesorge number. Similar behavior was observed by Weislogel and Ross.[7]

Velocity at the Centerline

An example of the depth of influence of the free surface oscillations is displayed in Fig. 14, where axial velocities at four locations along the cylinder axis ($r = 0$) are plotted, $Oh = 0.0110$, $\theta_{stat} = 51$ deg, and $\gamma = 0$, 10, and 100 cm^{-1}. Note that u_z is scaled as necessary to enhance observation. The location of the interface varies with time and thus the total depth of fluid along the centerline varies with time. A negative (u_z) velocity vector acts toward the cylinder base.

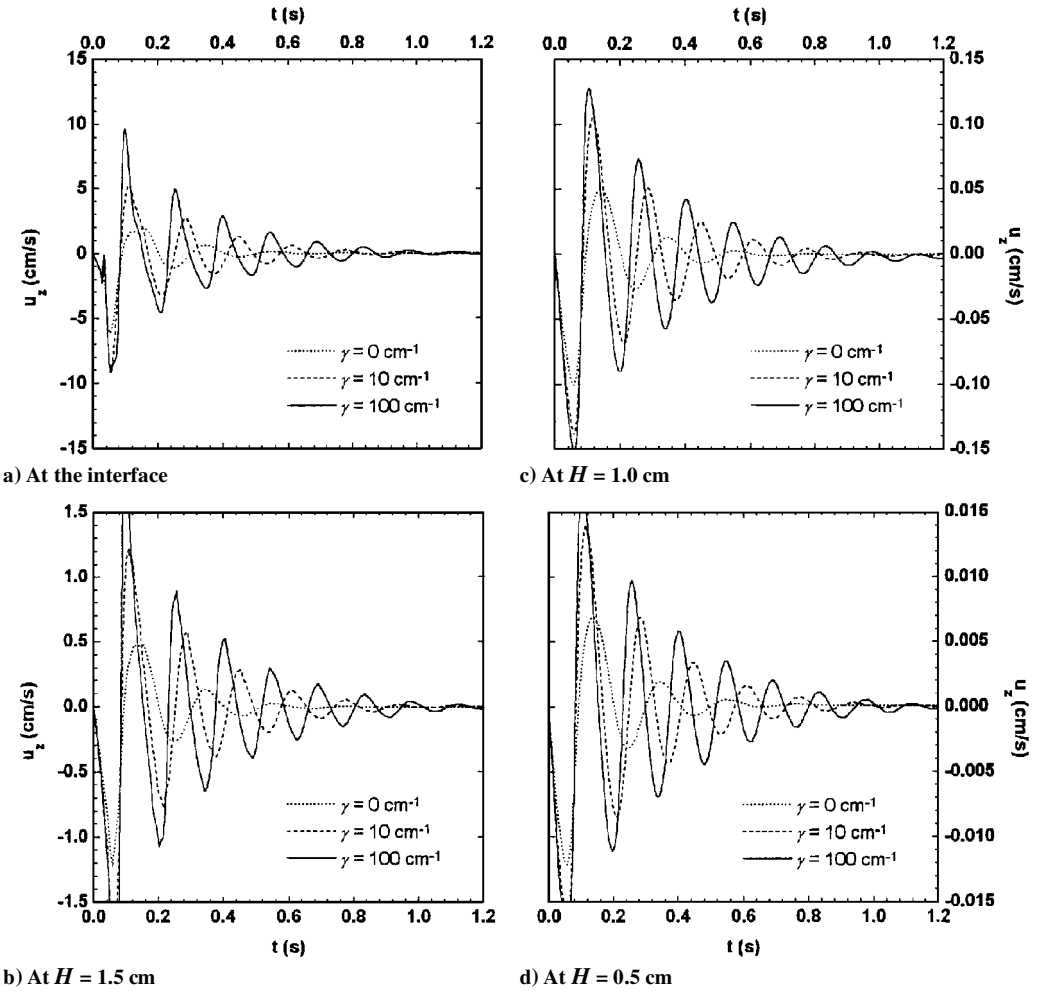

Fig. 14 Velocity histories for specific points along the centerline of the cylinder ($r = 0$) for $Oh = 0.0110$ with $\theta_{stat} = 51$ deg and varying γ.

Figure 14 shows the classic reduction of the damped oscillations with increasing depth. The amplitude and duration of these oscillations increase with increasing γ. Holding γ constant, the magnitude of the flow velocity along the centerline for any depth decreases with increasing Ohnesorge number. The velocities experienced along the cylinder axis are highest and off-axis values are increasingly damped as the wall is approached. In this test $H \sim 1.8R$ and velocity values at depths of $\sim 1.5R$ are approximately 1% of those present at the surface. A calculation was performed for an initial depth of 1.5 cm ($H \sim 1.5R$) for identical test parameters without effect to the resulting resonant frequency and settling time.

Comparison with Experiment

The utility of the hysteresis parameter boundary condition may be assessed by comparisons of the variety of numerical results for this test problem with those obtained experimentally by Weislogel and Ross.[7] Because the cell size, fluid properties, and contact angles were selected for such eventual comparisons, the settling time t_s and the frequency of oscillation ω_r serve well this purpose, as these were measured.[7] Because γ is a free parameter in the numerical study, it is of interest to see which value of γ best approximates the observed behavior of the bulk fluid. Insight into this best value of γ, here defined as γ_{real}, and its dependence on Oh and θ_{stat}, may prove useful as a tool to estimate γ a priori.

The approximate values of γ that seem to agree best with the data of Ref. 7 are listed in Table 2. Comparisons for the settling time are difficult due to the somewhat subjective determination of t_s used by Weislogel and Ross[7] to accommodate for experimental uncertainty. However, a general range of γ could be estimated from the numerical results that reproduced the experimentally measured values for $t_{s,exp}$ within $\pm 30\%$.

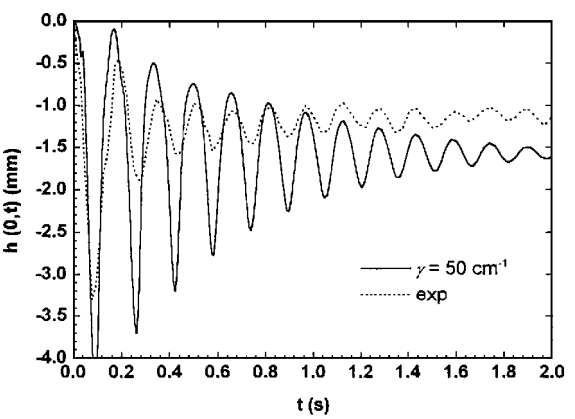

Fig. 15 Comparison of the numerical and experimental[7] results for the interface centerline location ($r = 0$); $Oh = 0.00222$, $\theta_{stat} = 44$ deg and for the calculations, $\gamma = 50$ cm^{-1}.

The hysteresis parameter γ_{real} was more easily identified for ω_r, and the numerical results agree well with the experiments. Figure 15 shows the experimental oscillation curve for the location of the meniscus centerline ($r = 0$) together with the numerical result for γ near γ_{real}. The liquid is silicone oil with $Oh = 0.00222$ and $\theta_{stat} = 44$ deg. Observation of the figure reveals a discrepancy between the final equilibrium configurations of the experimental and numerical tests. The numerical end state is correct as compared with the analytical solution.[15] Thus, the discrepancy is likely attributable to the experimental difficulties, as claimed by Weislogel and Ross,[7] of locating the initial axial location of the predominantly flat and thus blurred interface due to a narrow depth of field of the camera

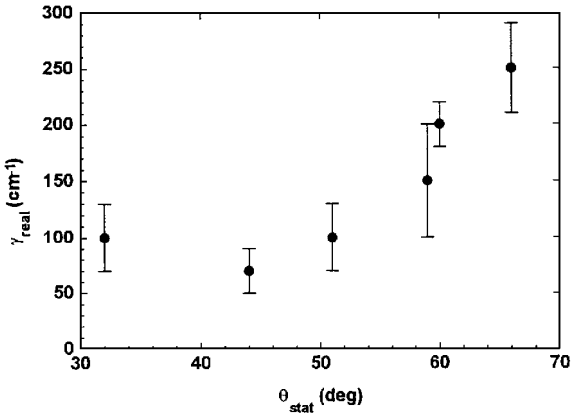

Fig. 16 Dependence of γ_{real} on the static contact angle θ_{stat}.

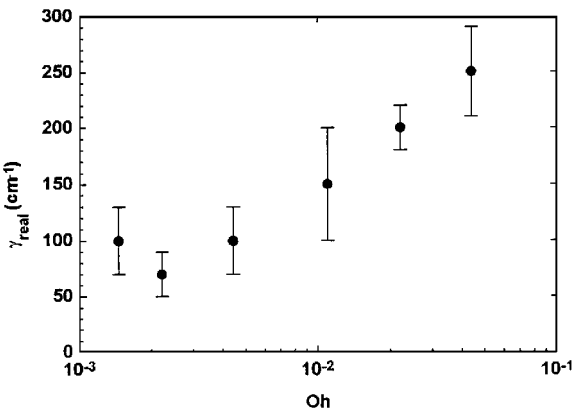

Fig. 17 Dependence of γ_{real} on the Ohnesorge number.

they employed. The settling time and frequency information are unaffected by the offset, which is always below ± 1 mm.

In Figs. 16 and 17, the selected values of γ_{real} for the various Ohnesorge numbers and static contact angle conditions are illustrated. It is not evident from the calculations whether the influence of Oh or θ_{stat} is stronger. Many additional runs would be necessary to provide full correlation of γ with respect to these parameters. The values for γ_0 listed in Table 2 predicted by the scale analysis [Eqs. (13–20)] when multiplied by 62 give a reasonable representation of γ_{real} found from the numerical results that best agreed with experiment. Thus, Eq. (20) may be modified to give

$$\gamma_0 \doteq 62 \frac{\cot(\theta_{stat}) - f(\theta_{stat}, Ca)}{f(\theta_{stat}, R)} \tag{24}$$

providing some correlation between γ_0 and γ_{real}. The scale values used in the calculation reproduce the experimentally determined values for $\omega_{r,exp}$ to within $\pm 5\%$. As an example of the utility of this result, it is found for the case of $Oh = 0.00442$ and $\theta_{stat} = 51$ deg that $\omega_r = 30.8$, 43.1, and 43.9 Hz for the values of $\gamma = 0$, γ_0, and ∞, respectively. For this case, $\omega_{r,exp} = 43.3$ Hz. Thus the use of γ_0 yields a more precise result within the anticipated bounding values of when $\gamma = 0$ and ∞.

Concluding Remarks

Numerical investigations on the damped oscillations of a liquid/gas interface after a step reduction in gravity were carried out using a commercial code. The results reveal the significance of the boundary condition at the moving contact line for numerically computed surface oscillations. The boundary condition imposed on the calculations incorporates a modified dynamic contact line/angle condition from which the hysteresis parameter γ arises as an adjustable parameter. Agreement with experimental results for this test problem are favorable for certain values of γ. The hysteresis parameter is correlated with the resonant frequency ω_r and the settling time t_s for a variety of Ohnesorge numbers Oh and static contact angles θ_{stat}. In each case, ω_r and t_s are minimized for $\gamma = 0$ and maximized as $\gamma \to \infty$. The terms ω_r and t_s are found to increase with increasing Oh and θ_{stat}. Concerning t_s, it was found that, for values of $\gamma \geq 100$ cm^{-1}, further dependence of t_s on γ is weak and t_s approaches a constant value. Similar behavior was observed for ω_r. In contrast to ω_r, the influence of θ_{stat} on t_s is weak. A comparison of the numerical results with the experiments of Weislogel and Ross[7] shows the dependence of a realistic hysteresis parameter γ_{real} on the Ohnesorge number and the static contact angle.

Acknowledgments

This work was supported by the German Space Agency (DARA) and was performed in cooperation with NASA Lewis Research Center in Cleveland, Ohio. The authors acknowledge R. Balasubramaniam for helpful discussions in connection with the subject of this work.

References

[1]Thulasiram, R. K., Sankar, T. S., and Vatistas, G. H., "A Study of the Behavior of Liquid Free Surface Due to Draining Under Microgravity Conditions," *Fluid Mechanics Phenomena in Microgravity*, AMD-Vol. 154/FED-Vol. 142, American Society of Mechanical Engineers, 1992, pp. 47–59.

[2]Bowman, T. E., "Cryogenic Liquid Experiments in Orbit, Vol. 1: Liquid Settling and Interface Dynamics," NASA CR-651, 1965.

[3]Rider, W. J., Kothe, D. B., Mosso, S. J., Cerutti, J. H., and Hochstein, J. I., "Accurate Solution Algorithms for Incompressible Multiphase Flow," AIAA Paper 95-0699, 1995.

[4]Dussan V., E. B., "On the Spreading of Liquids on Solid Surfaces: Static and Dynamic Contact Lines," *Annual Review of Fluid Mechanics*, Vol. 11, 1979, pp. 371–400.

[5]Hocking, L. M., "The Damping of Capillary-Gravity Waves at a Rigid Boundary," *Journal of Fluid Mechanics*, Vol. 179, 1987, pp. 253–266.

[6]Kamotani, Y., Chao, L., Ostrach, S., and Zhang, H., "Effect of g Jitter on Free-Surface Motion in a Cavity," *Journal of Spacecraft and Rockets*, Vol. 32, No. 1, 1995, pp. 177–183.

[7]Weislogel, M. M., and Ross, H. D., "Surface Reorientation and Settling in Cylinders upon Step Reduction in Gravity," *Microgravity Science and Technology*, Vol. 3, No. 1, 1990, pp. 24–32.

[8]Siegert, C. E., Petrash, D. A., and Otto, E. W., "Time Response of Liquid-Vapor Interface After Entering Weightlessness," NASA TN D-2458, 1964.

[9]Ross, H. R., and Pline, A. D., "Equilibrium Times for Gas-Liquid Systems Exposed to Step Changes in Gravity," American Inst. of Chemical Engineers Annual Meeting, Washington, DC, Dec. 1988.

[10]Young, G. W., and Davis, S. H., "A Plate Oscillating Across a Liquid Interface: Effects of Contact-Angle Hysteresis," *Journal of Fluid Mechanics*, Vol. 174, 1987, pp. 327–356.

[11]Cocciaro, B., Faetti, S., and Festa, C., "Experimental Investigation of Capillarity Effects on Surface Waves: Non-Wetting Boundary Conditions," *Journal of Fluid Mechanics*, Vol. 246, 1993, pp. 43–66.

[12]Ting, C. L., and Perlin, M., "Boundary Conditions in the Vicinity of the Contact Line at a Vertically Oscillating Upright Plate: An Experimental Investigation," *Journal of Fluid Mechanics*, Vol. 295, 1995, pp. 263–300.

[13]Satterlee, H. M., and Reynolds, W. C., "The Dynamics of the Free Liquid Surface in Cylindrical Containers Under Strong Capillary and Weak Gravity Conditions," Dept. of Mechanical Engineering, Stanford Univ., TR LG-2, Stanford, CA, 1964.

[14]Chao, L., Kamotani, Y., and Ostrach, S., "G-Jitter Effects on the Capillary Surface Motion in an Open Container Under Weightless Condition," *Fluid Mechanics Phenomena in Microgravity*, AMD-Vol. 154/FED-Vol. 142, American Society of Mechanical Engineers, 1992, pp. 133–143.

[15]Concus, P., "Static Menisci in a Vertical Right Circular Cylinder," *Journal of Fluid Mechanics*, Vol. 34, No. 3, 1968, pp. 481–495.

[16]Jiang, T. S., Oh, S. G., and Slattery, J. C., "Correlation for Dynamic Contact Angle," *Journal of Colloid and Interface Science*, Vol. 69, No. 1, 1979, pp. 74–77.

[17]Anon., "FIDAP (Fluid Dynamics Analysis Package) 7.0 Manual," Fluid Dynamics International Inc., Evanston, IL, 1993.

[18]Huh, C., and Mason, S. G., "The Steady Movement of a Liquid Meniscus in a Capillary Tube," *Journal of Fluid Mechanics*, Vol. 81, No. 3, 1977, pp. 401–419.

[19]Lowndes, J., "The Numerical Simulation of the Steady Movement of a Fluid Meniscus in a Capillary Tube," *Journal of Fluid Mechanics*, Vol. 101, No. 3, 1980, pp. 631–646.

[20]Dussan V., E. B., and Davis, S. H., "On the Motion of a Fluid-Fluid Interface Along a Solid Interface," *Journal of Fluid Mechanics*, Vol. 65, 1974, pp. 665–684.

A. C. Tribble
Associate Editor